

Received: 03.12.2023

Accepted: 24.03.2024

Research Article

***A DFT-D investigation of the energetic and structural aspects of dehydrogenation of methanol on a bimetallic surface PtGe(110) exploring the germanium effect on the anti-poisoning of pt(110) catalytic activity***

Abdellatif Hassak <sup>a, 1</sup>, Rachida Ghailane <sup>a, 2</sup>

<sup>a</sup>Laboratory of Organic Chemistry, Catalysis and Environment, Theoretical Chemistry and Modeling unit. University of Ibn Tofail, Faculty of Sciences, Po Box 133, 14000 Kenitra. Morocco

**Abstract:** Platinum is the most active pure metal for dehydrogenating methanol to create hydrogen, which is crucial for fuel cells. However, one significant disadvantage that reduces the effectiveness and long-term performance of platinum catalysts is their susceptibility to CO poisoning. In the current study, we examine and elucidate the promotional impact of Ge on Pt catalysts with increased resistance to deactivation by CO poisoning. We do this by combining partial density of states calculations with electronic configuration and Mulliken atomic charges. The self-consistent periodic density functional theory with dispersion correction (DFT-D) was used to investigate the methanol adsorption and dehydrogenation mechanisms on the surface of PtGe (110). On the surface, several adsorption mechanisms of pertinent intermediates were found. Furthermore, a thorough analysis of a reaction network comprising four reaction paths revealed that, in terms of activation barriers, the first O—H bond scission of CH<sub>3</sub>OH appears to be more advantageous than C—H bond cleavage on the PtGe(110) surface. Additionally, it has been demonstrated that the main route on the PtGe(110) surface is CH<sub>3</sub>OH→CH<sub>3</sub>O→CH<sub>2</sub>O→CHO→CO evolution. The remarkable differences in the predominant reaction pathway on the Pt(110) surface, and PtGe(110) surface indicate that the Ge-doped Pt Nano catalyst is more selective and resistant to deactivation.

**Keywords:** Methanol dehydrogenation, Adsorption, DFT-D, DOS, PtGe(110) surface.

## 1. Introduction

Since the initial discovery of fossil fuels (including oil, coal, etc.), their utilization has surged at an alarming rate, hastening their depletion over time. This accelerated extraction process not only contributes to environmental degradation but also releases harmful pollutants such as CO<sub>2</sub> during combustion, exacerbating the greenhouse effect and directly impacting ecosystem balance. Consequently, the urgent quest for alternative, less environmentally detrimental energy sources poses a significant challenge for scientific inquiry. Moreover, the transportation sector emerges as a primary contributor to air quality deterioration, with a majority of vehicles equipped with internal combustion engines reliant on gasoline or diesel fuel. Notably, global fossil fuel consumption within

the transportation sector continues to escalate unabated [1-3].

Within this framework, various green energy sources, such as wind, solar, hydro, second-generation biofuel, etc., are being advocated as alternatives. Among these alternatives, the direct methanol fuel cell (DMFC) emerges as a viable solution to supplant fossil fuels. This technology holds promise due to its efficient conversion of chemical energy from methanol into electrical energy, boasting high power generation efficiency, density, and minimal pollutant emissions [4-6]. Furthermore, methanol's widespread availability is complemented by its advantageous characteristics stemming from its straightforward molecular structure and intriguing electrochemical properties. Consequently, it has garnered significant attention in numerous studies centered on its electro-

<sup>1</sup> Corresponding Authors

e-mail: [hassak.abdellatif@yahoo.fr](mailto:hassak.abdellatif@yahoo.fr)

<sup>2</sup> Corresponding Authors

e-mail: [ghailane\\_r@yahoo.fr](mailto:ghailane_r@yahoo.fr)

oxidation facilitated by platinum-based catalysts [7-9]. Additionally, harnessing H<sub>2</sub> generated in situ from the electro-catalytic breakdown of methanol offers several advantages compared to directly using pure H<sub>2</sub> as a green fuel. These benefits include enhanced transportability, storability, cost-effectiveness, and theoretical energy density. Moreover, in all fuel cell applications, the catalyzed reaction of alcohol significantly influences efficiency parameters, such as lifespan, reusability, and catalytic performance. To date, numerous studies have investigated the use of transition metals as catalysts in this context [13-15].

Given its exceptional activity, platinum is frequently employed as an electro-catalyst for the methanol oxidation reaction (MOR) [16]. However, the primary challenges associated with utilizing platinum catalysts in direct methanol fuel cells (DMFCs) arise from the adsorption poisoning of CO and analogous intermediates formed during methanol dehydrogenation. This phenomenon diminishes the efficacy of catalysts by impairing their active sites and impeding the kinetics of methanol oxidation.

While fuel cells utilizing platinum in the anode section exhibit excellent performance, a significant impediment persists due to the prohibitively high cost of platinum for commercial viability. To address this challenge, several studies propose doping platinum with more cost-effective metals, alloys, or mixtures [17-28]. Consequently, numerous scientists have expressed considerable interest in conducting experimental and theoretical investigations concerning the dehydrogenation of methanol on platinum-based bimetallic catalysts, including PtSn, PtPb, PtNi, PtAu, PtPd, and PtMo [29-34]. Research indicates that the Pt-ligand alloy enhances electro-catalytic performance compared to monometallic catalysts, attributed to ligand and ensemble effects [35]. However, limited studies have explored platinum-based clusters to demonstrate germanium-doped platinum's improved catalytic activity and anti-poisoning effects. According to Elisa Jimenez-Izal et al., germanium is an optimal dopant for adjusting Pt selectivity. Consequently, the Pt-Ge alloy reduces the affinity of pure metal clusters towards alkenes, thereby promoting their desorption. Additionally, germanium substantially decreases carbon affinity, potentially enhancing catalyst resistance to coking deactivation [36]. Another study explores the impact of alloying Pt with Ge, revealing that this combination results in catalysts with enhanced stability and increased resistance to CO poisoning [37]. Veizaga, N.S. et al. elucidated that platinum doping with germanium facilitates the conversion of CO to CO<sub>2</sub> and mitigates its poisoning effect compared to pure Pt usage [38]. The incorporation

of Ge induces electronic effects within the catalyst's metal phase, altering interactions between Pt and the Ge promoter. Notably, Natalia S. Veizaga et al. demonstrated the significant promotion of CO oxidation to CO<sub>2</sub> and higher electro-catalytic activity exhibited by the PtGe bimetallic catalyst in both CO stripping and DMFC experiments [39]. Understanding that germanium was chosen because of its specific surface area, which is crucial in the disciplines of adsorption and catalysis, and its electronic configuration, especially in the d band, which is in charge of the catalytic capabilities. Additionally, Ge is also more readily available and less expensive than platinum, which has an impact on the cost-effectiveness of producing hydrogen. Exploring the catalytic efficiency of the PtGe surface in methanol dehydrogenation presents an intriguing avenue for research. This process holds promise as a means to produce H<sub>2</sub>, potentially establishing it as a novel energy source.

The present work aims to investigate the methanol adsorption on the PtGe surface by taking into account the many intermediate derivatives that are involved in this process. The associated co-adsorption structures were also identified.

In addition, the activation barriers and energies of elementary reactions on the PtGe surface were evaluated in the context of the methanol dehydrogenation process. Specifically, the reaction pathways involving the initial C—H and O—H bond cleavages were investigated, and transition states were identified on the PtGe surface using the dispersion-corrected density functional theory (DFT-D) approach with the periodic slab model. Here, it was crucial to analyze how bimetallic PtGe catalysts influenced selective pathways and compare them to those on a Pt surface to propose an optimal reaction mechanism for methanol dehydrogenation. This novel theoretical study investigates how the efficiency of methanol dehydrogenation is influenced by introducing Ge into the Pt surface. This method offers the advantage of immediately utilizing the generated hydrogen in the electro-catalyst, potentially benefiting direct methanol fuel cells (DMFCs).

## 2. Computational Method

Based on the crystal geometric structure provided by the Material Studio database, the platinum mesh is once more optimized using the DMol3 program integrated within Material Studio [40, 41]. Then, a four-layer periodic slab with a p(4x4) super-cell (16 Pt atoms in the top layer, 9 in the second, 16 in the third, and 9 in the fourth) was constructed using the structure optimized by DMol<sup>3</sup>. To avoid interactions between periodic tiles, 15 Å of empty tile was placed perpendicular to the surface. The PtGe alloy is formed by substituting half of the Pt

atoms with Ge atoms solely in the top layer of the Pt(110) surface. In all computations conducted herein, the two lower layers of PtGe(110) atoms were kept fixed, while the upper two layers as well as the adsorbent were allowed to relax. The Perdew-Burke-Ernzerhof (PBE) functional within the generalized gradient approximation (GGA) was employed to compute the energy of valence electron exchange-correlation interactions in DFT-D calculations, which were performed using DMol<sup>3</sup> [42]. However, to accelerate the convergence a Fermi spread of 0.005 Ha was used, and to gain on the calculation cost and have good precision, several k-point sampling tests were considered the results showed that the minimum time of convergence and the minimum energy of the optimization of the geometry of the supercell corresponds to the point k 4x4x1 using the Monkhorst-Pack scheme [43]. To expand the valence electron functions into a set of numerical atomic orbitals, a dual numerical basis with polarization functions (DNP) was employed. Core processing was specified using the Density Functional Half Core Pseudo Potential (DSPP) to ensure calculations with both accuracy and efficiency. The global orbital cutoff was established at 4.6 Å, and DFT-D correction was applied to enhance accuracy. Van der Waals interactions, as well as hydrogen bonds, were corrected using Grimme's method [44, 45] provided in the DMol<sup>3</sup> module. The maximum force, maximum displacement, SCF tolerance, and energy, were the respective convergence standards for configuration optimization and energy calculation, and they were set at 0.002 Ha/Å, 0.005 Å,  $1.0 \times 10^{-6}$  Ha, and  $1.0 \times 10^{-5}$  Ha. At the same theoretical level as the whole LST/QST approach, the transition state (TS) search was carried out [46]. This approach involved maximizing the linear synchronous transit (LST) and then minimizing energy along directions aligned with the reaction route to approximate the transition state (TS). The approximated TS were employed to conduct a conjugate gradient minimization cycle subsequent to maximizing the quadratic synchronous transit (QST). This cycle iterated until a stationary point was localized. For TS searches, the convergence requirement for the

root mean square of the atomic forces was set at 0.01 Ha/Å.

When a molecule adsorbs onto the PtGe(110) surface, the adsorption energy is estimated using the following expression:

$$E_{\text{ads}} = E_{(\text{mol}/\text{PtGe}(110))} - E_{(\text{PtGe}(110))} - E_{\text{mol}} \quad (1)$$

Where  $E_{(\text{mol}/\text{PtGe}(110))}$  represents the combined total energy of the PtGe(110) surface and the adsorbed molecule,  $E_{\text{mol}}$  refers to the overall energy of the isolated molecule, and  $E_{(\text{PtGe}(110))}$  refers to the overall energy of the pure PtGe(110) surface. Negative values of adsorption energy ( $E_{\text{ads}}$ ) indicate an exothermic process, suggesting spontaneous interaction between the adsorbents and the surface [47].

The definition of the reaction energy  $E_r$  is:

$$E_r = E_{\text{FS}} - E_{\text{IS}} \quad (2)$$

The activation barrier  $E_a$  was calculated according to:

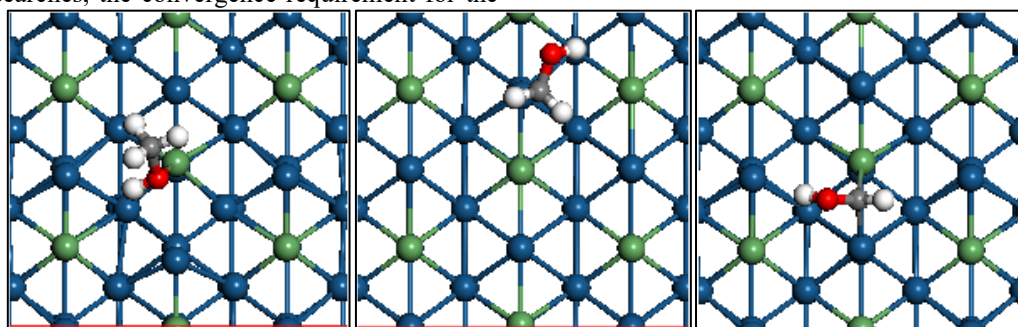
$$E_a = E_{\text{TS}} - E_{\text{IS}} \quad (3)$$

Where  $E_{\text{IS}}$ ,  $E_{\text{FS}}$ , and  $E_{\text{TS}}$  represent the initial, final, and transition states energies, respectively.

### 3. Results and discussion

#### 3.1. Structure optimization and estimation of adsorption energy for various key intermediates

In the entire methanol dehydrogenation cycle, there are a number of possible intermediates such as CH<sub>3</sub>OH, CH<sub>2</sub>OH, CH<sub>3</sub>O, CHO, CH<sub>2</sub>O, COH, HCO, CO, and H which have been considered in many theoretical works [48–50]. These intermediates can be divided into three categories: CH<sub>x</sub>OH (x = 0, 1, 2, 3), CH<sub>x</sub>O (x = 0, 1, 2, 3), and H. In this part, we have proposed the systematic study of MOR of all intermediate species to determine their favorable adsorption patterns on the PtGe(110) surface taking into account the following adsorption sites the top site ( $t_{\text{Pt}}$ ;  $t_{\text{Ge}}$ ), bridge site ( $b_{\text{PtPt}}$ ;  $b_{\text{GeGe}}$ ;  $b_{\text{PtGe}}$ ) and hollow site ( $h_{\text{Pt2Ge}}$ ;  $h_{\text{Ge2Pt}}$ ). The adsorption energies of methanol and all intermediates involved in the dehydrogenation are presented in Table 1, while the corresponding stable configurations are presented in figure 1.



Abdellatif Hassak, Rachida Ghailane

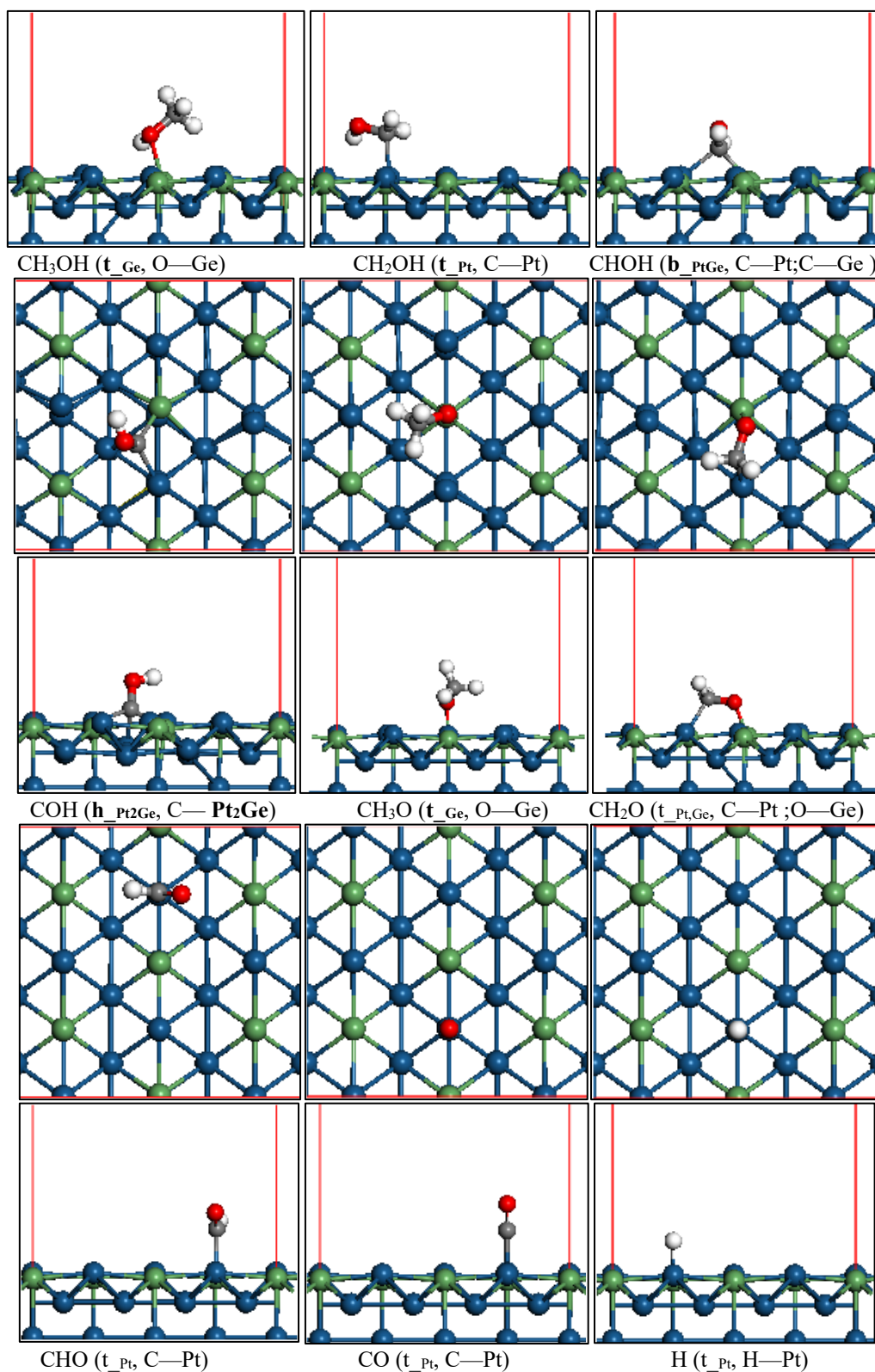


**Figure 1.** Most stable positions of intermediate species on the surface of PtGe(110) during the methanol dehydrogenation process. The colors Cyan, Green, Grey, Red and White represent Pt, Ge, C, O and H atoms respectively.

**Table 1.** Adsorption energies  $E_{ads}$  (in eV) and the main bond lengths of the intermediates involved in methanol dehydrogenation on the PtGe(110) surface considering all interactions of each species with various sites (top, bridge, and hollow). The results for the most stable positions are highlighted in bold characters.

Specie	Site of adsorption	Configuration	Bond length (Å)	$E_{ads}(eV)/$ PtGe(110)	$E_{ads}(eV)$ on other surface
CH <sub>3</sub> OH	t <sub>Pt</sub>	O—Pt	d <sub>O—Pt</sub> =2.292; d <sub>C—O</sub> =1.454	-0.897	$E_{ads}/Pt(110)$ = -0.95;top [51]
	t <sub>Ge</sub>	<b>O—Ge</b>	<b>d<sub>O—Ge</sub>=2.247;d<sub>C—O</sub>=1.457</b>	<b>-0.976</b>	$E_{ads}/Pt(111)$ = -0.456;top [52] $E_{ads}/Pt_3Cu(110)$ = -0.93;top(Cu) [51] $E_{ads}/PtRu(111)$ = -0.70;top(Ru) [53] $E_{ads}/PtPd_3(111)$ = -0.12;top(Pt) [54] $E_{ads}/PdGe(110)$ = -0.873;top(Pd) [55]
CH <sub>2</sub> OH	t <sub>Pt</sub>	<b>C—Pt</b>	<b>d<sub>C—Pt</sub>=2.071;d<sub>C—O</sub>=1.401</b>	<b>-2.476</b>	$E_{ads}/Pt(110)$ = -3.11;top [51]
	t <sub>Ge</sub>	C—Ge	d <sub>C—Ge</sub> =2.009;d <sub>C—O</sub> =1.439	- 2.340	$E_{ads}/Pt(111)$ = -2.166;top [52] $E_{ads}/Pt_3Cu(110)$ = -3.41;b(PtCu) [51] $E_{ads}/PtRu(111)$ = -2.14;B(RuRu) [53] $E_{ads}/PtPd_3(111)$ = -2.386;top(Pt) [54] $E_{ads}/PdGe(110)$ = -2.130;top(Ge) [55]
CHOH	t <sub>Pt</sub>	C—Pt	d <sub>C—Pt</sub> =1.896; d <sub>C—O</sub> =1.323	- 4.359	$E_{ads}/Pt(110)$ = -4.11;B(PtPt) [51]
	b <sub>PtGe</sub>	<b>C—Pt</b> C—Ge	<b>d<sub>C—Pt</sub>=2.096</b> <b>d<sub>C—Ge</sub>=2.008</b> <b>d<sub>C—O</sub>=1.366</b>	<b>- 4.438</b>	$E_{ads}/Pt_3Cu(110)$ = -4.24;top(Pt) [51] $E_{ads}/PtRu(111)$ = -3.58;B(RuRu) [53] $E_{ads}/PtPd_3(111)$ = -3.399;B(PtPt) [54] $E_{ads}/PdGe(110)$ = -3.885;B(PdPd) [55]
COH	h <sub>Pt2Ge</sub>	<b>C—Pt<sub>2</sub>Ge</b>	<b>d<sub>C—Pt</sub>=2.007</b> <b>d<sub>C—Pt</sub>=2.114</b> <b>d<sub>C—Ge</sub>=2.022</b> <b>d<sub>C—O</sub>=1.355</b>	<b>- 3.883</b>	$E_{ads}/Pt(110)$ = -5.50;B(PtPt) [51] $E_{ads}/PtCu(110)$ = -4.57;b(PtCu) [51] $E_{ads}/PtRu(111)$ = -4.75;H(PtRuRu) [53] $E_{ads}/PtPd_3(111)$ = -4.961;H(PtPtPt) [54] $E_{ads}/PdGe(110)$ = -3.023;B(PdPd) [55]
CH <sub>3</sub> O	t <sub>Pt</sub>	O—Pt	d <sub>O—Pt</sub> =2.017;d <sub>C—O</sub> =1.395	-2.209	$E_{ads}/Pt(110)$ = -2.89;b(PtPt) [51]
	t <sub>Ge</sub>	<b>O—Ge</b>	<b>d<sub>O—Ge</sub>=1.790;d<sub>C—O</sub>=1.430</b>	<b>-2.955</b>	$E_{ads}/Pt(111)$ = -1.669;b(PtPt) [52] $E_{ads}/Pt_3Cu(110)$ = -3.02;b(PtCu) [51] $E_{ads}/PtRu(111)$ = -2.26;b(RuRu) [53] $E_{ads}/PtPd_3(111)$ = -1.691;top(Pt) [54] $E_{ads}/PdGe(110)$ = -3.004;top(Ge) [55]
CH <sub>2</sub> O	t <sub>Pt,Ge</sub>	<b>C—Pt</b> <b>O—Ge</b>	<b>d<sub>C—Pt</sub>=2.082;d<sub>O—Ge</sub>=1.841</b> <b>d<sub>C—O</sub>=1.396</b>	<b>- 1.474</b>	$E_{ads}/Pt(110)$ = -1.53;b(PtPt) [51] $E_{ads}/Pt(111)$ = -0.508; b(PtPt) [52]
	t <sub>Pt,Ge</sub>	C—Ge O—Pt	d <sub>C—Ge</sub> =2.044;d <sub>O—Pt</sub> =2.044 d <sub>C—O</sub> =1.376	- 0.606	$E_{ads}/Pt_3Cu(110)$ = -1.32;b(PtCu) [51] $E_{ads}/PtRu(111)$ = -1.13;h(RuRuPt) [53] $E_{ads}/PtPd_3(111)$ = -0.333;b(PtPt) [54] $E_{ads}/PdGe(110)$ = -0.772;top(PdGe) [55]
CHO	t <sub>Pt</sub>	<b>C—Pt</b>	<b>d<sub>C—Pt</sub>=1.964;d<sub>C—O</sub>=1.208</b>	<b>- 2.756</b>	$E_{ads}/Pt(110)$ = -3.63;b(PtPt) [51]
	t <sub>Ge</sub>	C—Ge	d <sub>C—Ge</sub> =2.030;d <sub>C—O</sub> =1.210	- 1.921	$E_{ads}/Pt(111)$ = -2.452; b(PtPt) [52] $E_{ads}/Pt_3Cu(110)$ = -3.69;b(PtCu) [51] $E_{ads}/PtRu(111)$ = -2.70;b(RuRu) [53]

					$E_{ads}/PtPd_3(111) = -2.645; t(Pt)$ [54] $E_{ads}/PdGe(110) = -2.114; top(Pd)$ [55]
CO	$t_{Pt}$	C—Pt	$d_{C-Pt} = 1.875; d_{C-O} = 1.163$	- 1.528	$E_{ads}/Pt(110) = -2.50; b(PtPt)$ [51] $E_{ads}/Pt(111) = -1.741; h(PtPtPt)$ [52] $E_{ads}/Pt_3Cu(110) = -2.5; t(Pt)$ [51] $E_{ads}/PtRu(111) = -2.10; top(Ru)$ [53] $E_{ads}/PtPd_3(111) = -1.813; h(PtPtPt)$ [54] $E_{ads}/PdGe(110) = -1.366; b(PdPd)$ [55]
H	$t_{Pt}$ $t_{Ge}$	H—Pt H—Ge	$d_{H-Pt} = 1.564$ $d_{H-Ge} = 1.539$	- 2.712 - 2.255	$E_{ads}/Pt(111) = -2.788; h(PtPtPt)$ [52] $E_{ads}/PtRu(111) = -2.86; h(RuRuPt)$ [53] $E_{ads}/PtPd_3(111) = -2.948; h(PtPtPt)$ [54] $E_{ads}/PdGe(110) = -1.596; t(Pd)$ [55]

For the  $CH_xOH$  species series ( $x = 0, 1, 2, 3$ ), various configurations of adsorption at the top, bridge, and hollow were examined to determine the starting pattern of molecular adsorption of  $CH_3OH$  on  $PtGe(110)$  surface. According to our calculations, only the initial top configuration was found to be established and converged, methanol binds weakly to the top site ( $t_{Ge}$ ) of  $PtGe(110)$  via its oxygen atom such that the C—O axis is inclined by  $113.2^\circ$  relative to the surface normal ( Fig. 1). The adsorption energy computed is  $-0.976$  eV while that on  $Pt(110)$  is  $-0.95$  eV (Table 1). This structure is demonstrated by the fact that the methanol molecule is polar ( $mCH_3OH = 1.67$  D) with few negative charges concentrated on the oxygen side, giving  $CH_3OH$  the ability to adsorb onto metal surfaces via paired orbitals isolated O. The weak adsorption corresponds to the long distance  $d_{O-Ge} = 2.247$  Å in the adsorption configuration (figure 1).

The hydroxymethyl ( $CH_2OH$ ) is formed after the cleavage of the C—H bond in  $CH_3OH$ . The complete geometry optimization reveals that the top site  $t_{Pt}$  is the most stable adsorption site for  $CH_2OH$  species on  $PtGe(110)$ , with a bond distance of  $d_{C-Pt} = 2.071$  Å and  $d_{C-O} = 1.401$  Å and an adsorption energy of  $-2.476$  eV. In this most stable configuration which is also verified on other metal surfaces [33, 51], the C—O bond of  $CH_2OH$  is nearly parallel to the Pt—Ge bond. The proximity of the methylene and hydroxyl H atoms to the  $PtGe(110)$  surface facilitates their activation.

The dehydrogenation intermediate product,  $CHOH$ , could bind stably at the bridge site ( $b_{PtGe}$ ) over the  $PtGe(110)$  surface, with a very large adsorption energy of  $-4.438$  eV it is better than that on  $Pt(110)$  ( $-4.11$  eV) [51], and  $PdGe(110)$  ( $-3.885$  eV) [55]. Through its C atom binding to atoms Pt and Ge of  $PtGe(110)$  surface with  $d_{C-Pt}$ ,  $d_{C-Ge}$ , and  $d_{C-O}$  of 2.096, 2.008, and 1.366 Å

respectively (figure 1). The entire  $CHOH$  atoms were in the same plane, which was perpendicular to the metal surface. The carbon atom in this geometric arrangement was orientated over a bridge site  $b_{PtPt}$  and tightly linked to O, H, and two neighboring Pt atoms via  $sp^3$  hybridization. On the surfaces of  $Pt(110)$  [51],  $PtRu(111)$  [53],  $PtPd_3(111)$  [54], and  $PdGe(110)$  [55], similar bridge site and geometrical configuration findings for  $CHOH$  were reported.

Hydroxymethylidyne (COH) prefers to bind to hollow site  $h_{Pt_2Ge}$  through its carbon atom with an adsorption energy of  $-3.883$  eV, and the bond lengths  $d_{C-Pt}$ ,  $d_{C-Pt}$ ,  $d_{C-Ge}$ , and  $d_{C-O}$  are 2.007, 2.114, 2.022, and 1.355 respectively. View that the C atom has no neighbor H, the interaction of the surface and the C atom is strong, but it is less than that on  $PtRu(111)$  [53]  $PtPd_3(111)$  [54]  $PtCu(110)$  [51]  $Pt(110)$  [51] which facilitates its dehydrogenation compared to other surfaces.

The second category of  $CH_xO$  ( $x = 0, 1, 2, 3$ ) species arises after O—H bond cleavage, followed by subsequent C—H abstractions on the  $PtGe(110)$  surface. Similar to methanol, methoxy ( $CH_3O$ ) prefers to adsorb at the top site  $t_{Ge}$  with a bond length of  $d_{O-Ge} = 1.790$  Å. The C—O axis forms an angle of  $121.9^\circ$  with the surface normal, and the O—Ge axis tends to be vertical to the surface, like that of methanol. This configuration gives an adsorption energy of  $-2.955$  eV (Table 1) similar to that on  $PdGe(110)$ , which has an adsorption energy of  $-3.004$  eV [55].

It is commonly acknowledged that formaldehyde ( $CH_2O$ ) tends to be adsorbed by an adsorption mode in which both C and O atoms bind to the surface [56]. We explored various adsorption configurations of  $CH_2O$  on the  $PtGe(110)$  surface, including the top ((C—Pt, O—Ge), (C—Ge, O—C)) bridge and hollow sites. According to our calculated results, the two structures of the summit

have been acquired. This is consistent with the mode of adsorption where  $\text{CH}_2\text{O}$  binds to the surface via O and C atoms simultaneously [37]. the most stable structure on the PtGe(110) surface is where  $\text{CH}_2\text{O}$  adsorbs on  $t_{\text{Pt,Ge}}$  such that the C atom binds to the Pt atom and the O atom binds to the Ge atom with bond lengths  $d_{\text{C-Pt}}=2.082\text{\AA}$ ,  $d_{\text{O-Ge}}=1.841\text{\AA}$ , and adsorption energy - 1.474 eV (Table 1, figure 1).

When CHO is adsorbed on the PtGe(110) surface, a modification occurs. It is the C—Pt bond rather than the O—Pt bond which connects the intermediate to the surface, with an adsorption energy that is substantially enhanced and equals - 2.756 eV, which is beneficial for the subsequent dehydrogenation reaction. The distances of the C—O and C—Pt bonds are respectively 1.208 Å and 1.964 Å.

Regarding carbon monoxide, its high adsorption often leads to catalyst poisoning, particularly in catalysts composed of Pt metal. CO exhibits modest adsorption on the surface of PtGe(110), with an adsorption energy that is estimated to be -1.528 eV less than that of Pt(110) [51]. We explored several configurations positioned at the top, bridge, and hollow sites to determine the most optimal structure and associated adsorption energy. The findings show that CO has the maximum binding energy and attaches vertically to the metal surface via the C—Pt bond.

We also examined the adsorption of hydrogen (H) at various sites on the surface. With adsorption energy of -2.712 eV, the top site ( $t_{\text{Pt}}$ ) emerges as the most favored location for the H atom. The H—Pt bond length measures approximately 1.564 Å.

In general, a comparison between the results obtained for the adsorption of methanol and various

intermediates on the surface of PtGe(110) in this study and those obtained on the Pt(110) surface [51] from the literature reveals distinct behaviors. Specifically, Pt(110) and PtGe(110) exhibit significant differences during the adsorption of intermediates involved in the methanol dehydrogenation process. For  $\text{CH}_3\text{OH}$ ,  $\text{CH}_3\text{O}$ , and  $\text{CH}_2\text{O}$ , their adsorptions show minimal change with the addition of Ge. As indicated in Table 1, the common feature of these adsorptions is their association with O—Ge bonds. However, the adsorptions of  $\text{CH}_2\text{OH}$ ,  $\text{CHOH}$ ,  $\text{CHO}$ , and  $\text{CO}$  weaken with the addition of Ge. Moreover,  $\text{COH}$  adsorption experiences a substantial decrease with the inclusion of Ge. This discrepancy suggests potential selectivity differences between Pt(110) and PtGe(110) in the production of the  $\text{COH}$  intermediate. Through these calculations, it is evident that the addition of Ge in Pt could mitigate catalyst poisoning. Furthermore, the significantly lower adsorption energy of  $\text{CO}$  (-1.528 eV for PtGe(110) versus -2.50 eV for Pt(110)) [51] underscores the long-term stability attribute of Ge-doped platinum catalysts. The presence of Ge in the alloy contributes to enhancing the anti-poisoning properties of the PtGe alloy system, a phenomenon also observed and studied by other researchers [36-38].

In order to explain the effect of platinum-germanium doping, the density of the state of a Pt atom of the Pt(110) surface and the PtGe(110) surface was calculated and presented in figure 2. In addition, due to the periodicity of the system, the atomic charges of some atoms chosen from the upper surface and the one just adjacent to the bottom of Pt(110) and PtGe(110) surfaces are calculated and listed in Table 2.

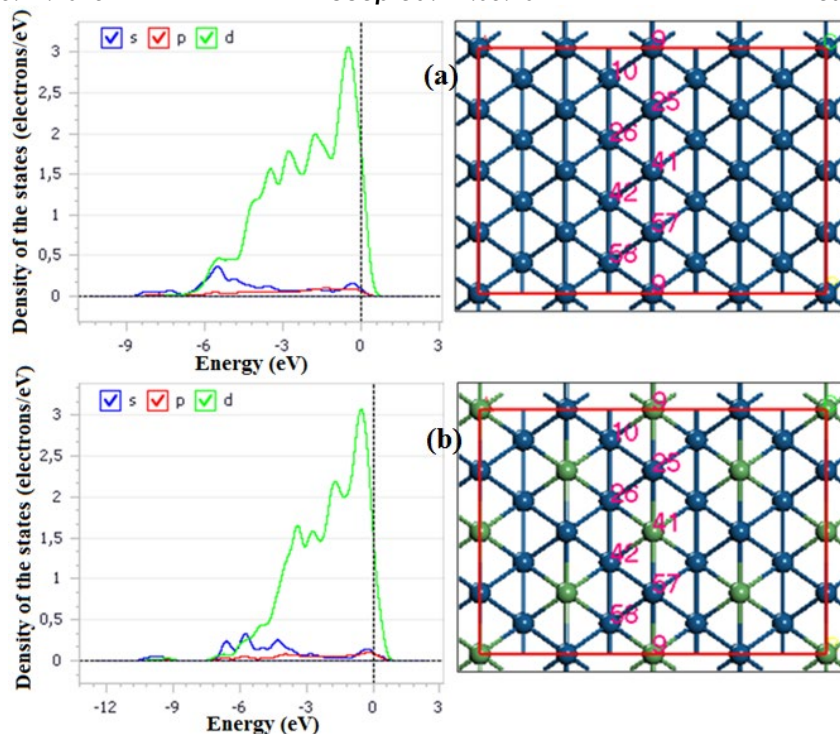


**Figure 2.** (a) Partial density of states of a Pt atom of the Pt(110) surface; (b) Partial density of states of a Pt atom of the PtGe(110) surface.

**Table 2.** Electronic configuration, Mulliken atomic charges of Ge and Pt in different metallic

Atom <sup>(a)</sup>	Electronic configuration <sup>(a)</sup>			Charge <sup>(a)</sup>
Pt(9)	s(2.938)	p(6.389)	d(8.644)	0.029
Pt(10)	s(2.922)	p(6.564)	d(8.543)	-0.029
Pt(25)	s(2.938)	p(6.389)	d(8.645)	0.028
Pt(26)	s(2.922)	p(6.564)	d(8.543)	-0.029
Atom <sup>(b)</sup>	Electronic configuration <sup>(b)</sup>			Charge <sup>(b)</sup>
Ge(9)	s(1.790)	p(1.578)	d(10.317)	0.315
Pt(10)	s(2.917)	p(6.559)	d(8.613)	-0.089
Pt(25)	s(2.933)	p(6.393)	d(8.709)	-0.036
Pt(26)	s(2.917)	p(6.559)	d(8.613)	-0.089

<sup>(a)</sup> Pt(110) surface; <sup>(b)</sup> PtGe(110) surface.

The interaction of carbon monoxide with transition metals is through the formation of a metal-carbon  $\sigma$  bond via the donation of a lone pair from the carbon to the vacant d orbitals, and also by back donation of  $\pi$  electrons from the d-metal filled orbitals to the anti-bonding CO  $\pi$  orbital.

In the electronic structures of the atoms(Pt(10), Pt(25), Pt(26)), it is clear that there is an electronic transition that occurs mainly from 6s to 5d in the Pt atoms after the addition of Ge (figure 2) and (Table 2). Moreover, the Pt atoms carry more negative (or

less positive) charge in the Ge-doped PtGe(110) surface than in the pure Pt(110) surface, indicating an overall charge transfer from Ge to Pt (Table 2). In the bimetallic surface, the charge transfer from Ge to Pt leads to an increase in the electron density in the Pt 5d orbit. The change in the electronic structure of Pt counteracts the charge transfer from orbital CO 5 $\sigma$  to Pt, weakening CO adsorption and thus mitigating CO poisoning, this is in good agreement with the results obtained by Natalia S et al. [38]. These results translate into the adsorption

energy of CO on the PtGe(110) surface which is equal to  $E_{ads}/PtGe(110) = -1.528$  eV it is lower than that obtained on the Pt(110) surface  $E_{ads}/Pt(110) = -2.50$  eV [51]. A low density of states at the Fermi level (figure 2) could reduce the Pt-CO bond energy to enhance the catalytic activity for methanol decomposition [57,58].

### 3.2. Co-adsorption configurations and the energy of important intermediates and hydrogen on the PtGe(110) surface

Examining and researching the most stable locations of co-adsorption intermediates and hydrogen on the PtGe(110) surface—[CH<sub>3</sub>O+H], [CH<sub>2</sub>OH+H], [CH<sub>2</sub>O+H], [CHOH+H], [CHO+H], [COH+H], and [CO+H]—is necessary to understand the process of methanol CH<sub>3</sub>OH dehydrogenation on the surface of PtGe(110).

Figure 2 shows all of the optimum co-adsorbed configurations. Table 3 lists the associated adsorption sites, co-adsorption energy, and the total of the separated adsorption energies. The following definition applies to the co-adsorption energies between correlative species on the PtGe(110) surface:

$$E_{coads} = E_{A+B/PtGe(110)} - E_{PtGe(110)} - E_A - E_B \quad (4)$$

Where  $E_{A+B/PtGe(110)}$ ,  $E_{PtGe(110)}$ ,  $E_A$ ,  $E_B$  represent the total energies for the co-adsorbed (A+B)/PtGe slab systems, the (4×4) supercell of the PtGe slab, and the respective free molecules of A and B [55]. In this section, all calculations are performed for the initial co-adsorption configuration on the Pd(110) surface, with the corresponding entities placed at the adjacent and most steady adsorption sites.

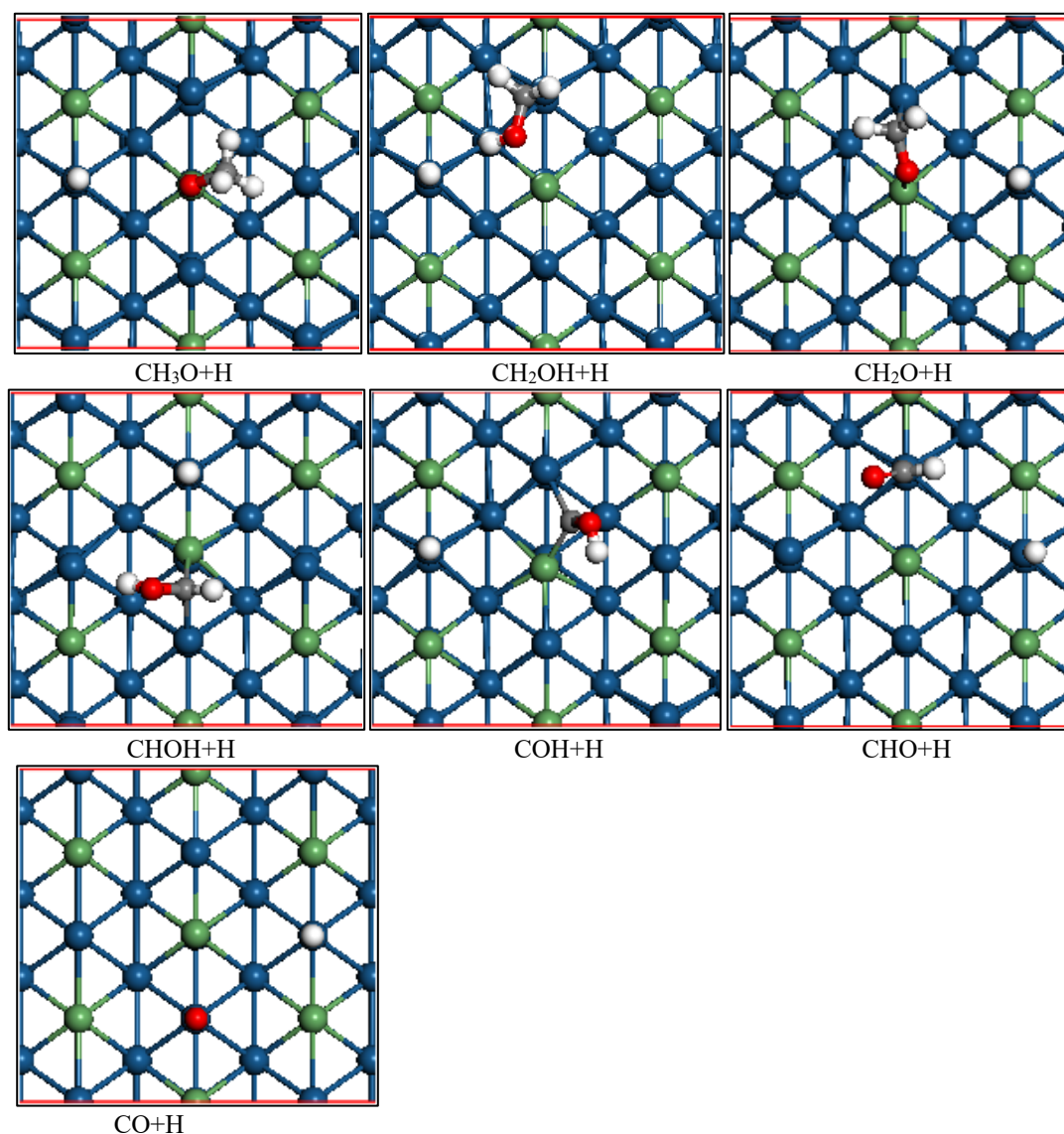


**Figure 3.** The most stable positions of intermediate species and hydrogen atom co-adsorbed on the PtGe(110) surface

**Table 3.** Most stable co-adsorption structures, co-adsorption energies and the sum of separate adsorption energies (eV).

Intermediates and hydrogen specie	favorable adsorption sites	$E_{Co-ads}$ (in eV)	Sum of separated $E_{ads}$ (in eV)
CH <sub>3</sub> O+H	t <sub>Ge</sub> + t <sub>Pt</sub>	-5.771	-5.667
CH <sub>2</sub> OH+H	t <sub>Pt</sub> + t <sub>Pt</sub>	-5.390	-5.188
CH <sub>2</sub> O+H	t <sub>Pt,Ge</sub> + t <sub>Pt</sub>	-4.176	-4.186
CHOH+H	b <sub>PtGe</sub> + t <sub>Pt</sub>	-5.583	-5.468
CHO+H	t <sub>Pt</sub> + t <sub>Pt</sub>	-7.142	-7.15
COH+H	h <sub>Pt2Ge</sub> + t <sub>Pt</sub>	-6.530	-6.595
CO+H	t <sub>Pt</sub> + t <sub>Pt</sub>	-4.530	-4.540

An important factor in the dehydrogenation of methanol is co-adsorption. As shown in figure 3, the most stable co-adsorbed configurations namely [CH<sub>3</sub>O+H], [CH<sub>2</sub>OH+H], [CH<sub>2</sub>O+H], [CHOH+H], [CHO+H], [COH+H], and [CO+H], have been optimized. Table 3 analysis reveals that the H atom is adsorbed at the neighboring top site t<sub>Pt</sub> (figure 3), and all of the optimal co-adsorption configurations maintain the initial equilibrium states of the CH<sub>3</sub>O, CH<sub>2</sub>OH, CH<sub>2</sub>O, CHOH, CHO,

COH, and CO species. The outcomes obtained accord well with previous computations published in the literature [54]. However, the observed discrepancy between the sum of the individual adsorption energies and the co-adsorption energies predicted for the species [CH<sub>3</sub>O+H], [CH<sub>2</sub>OH+H], [CH<sub>2</sub>O+H], [CHOH+H], [CHO+H], [COH+H], and [CO+H] on PtGe(110) respectively, suggests that there is interaction energy between the species.

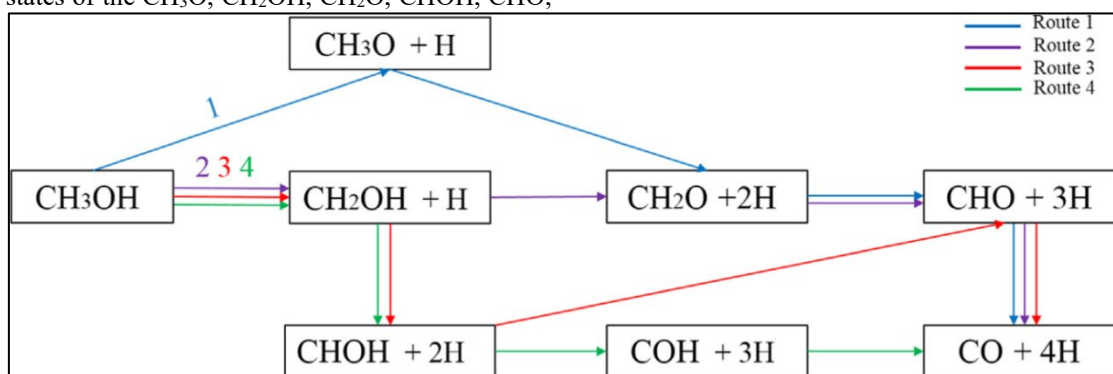


**Figure 4.** Different routes of methanol dehydrogenation

**Table 4.** Dehydrogenation reactions from CH<sub>3</sub>OH to CO+H on PtGe(110) surface

Route(1)	Route(2)	Route(3)	Route(4)
CH <sub>3</sub> OH→CH <sub>3</sub> O+H	CH <sub>3</sub> OH→CH <sub>2</sub> OH+H	CH <sub>3</sub> OH→CH <sub>2</sub> OH+H	CH <sub>3</sub> OH→CH <sub>2</sub> OH+H
CH <sub>3</sub> O→CH <sub>2</sub> O+H	CH <sub>2</sub> OH→CH <sub>2</sub> O+H	CH <sub>2</sub> OH→CHOH+H	CH <sub>2</sub> OH→CHOH+H
CH <sub>2</sub> O→CHO+H	CH <sub>2</sub> O→CHO+H	CHOH→CHO+H	CHOH→COH+H
CHO→CO+H	CHO→CO+H	CHO→CO+H	COH→CO+H

### 3.3. Dehydrogenation route of CH<sub>3</sub>OH on PtGe(110) surface

The diversity of intermediates could give rise to many possible reaction pathways in the dehydrogenation of methanol at the surface of PtGe(110) figure 4. Since in the dehydrogenation of CH<sub>3</sub>OH to CO, four C—H bonds and one O—H bond must be cleaved afterward. The corresponding reactions are listed in Table 4. Two main modes are considered, C—H mode and O—H mode:

i-- The first pathway initiates with the breaking of the O—H bond is succeeded by a series of

successive C—H bond cleavages leading to the formation of CO. Table 5 displays the energy activation and reaction energies for each elementary step, while the corresponding states of transition (TS) for these essential reactions are illustrated in figure 5.

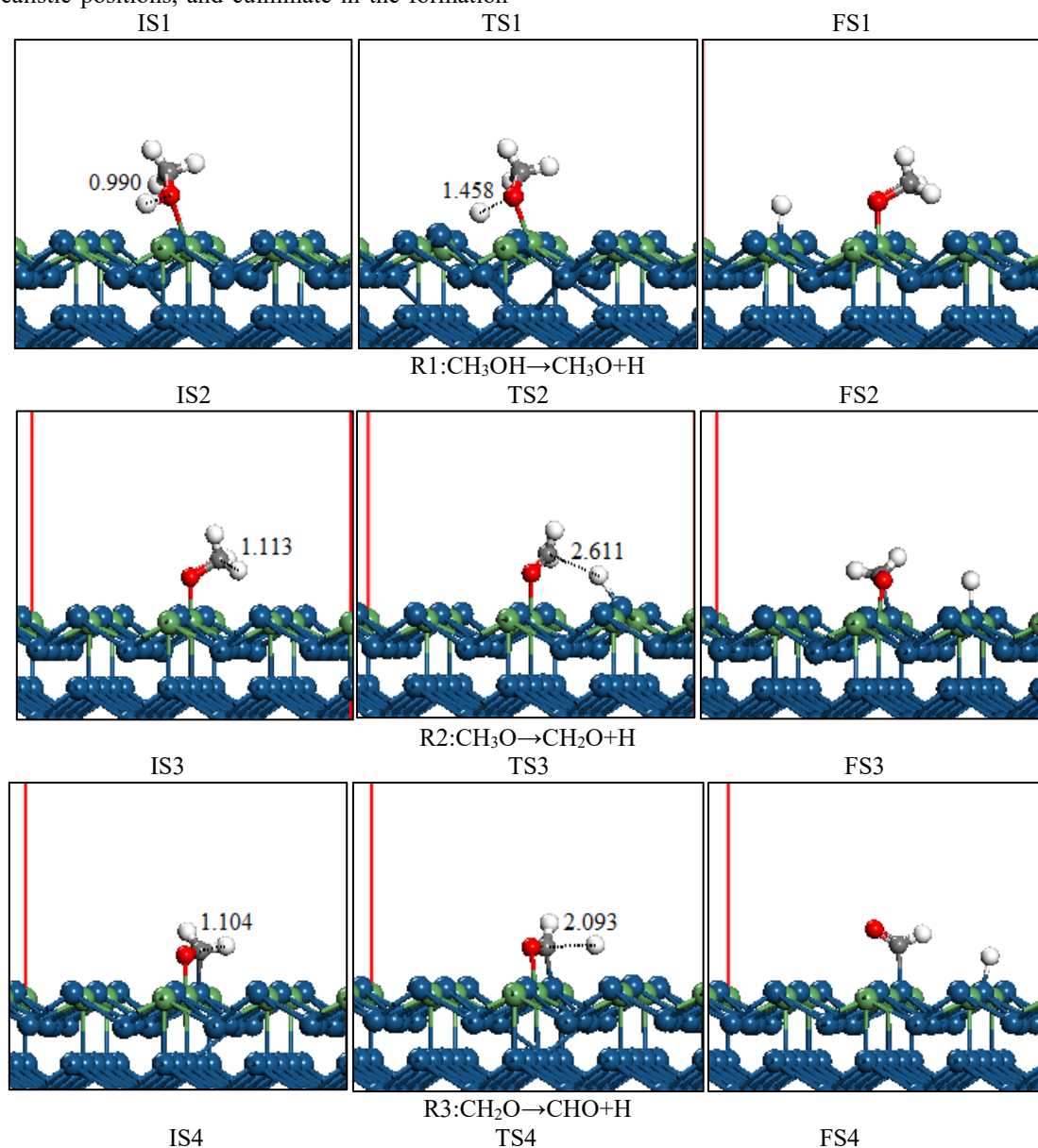
ii-- The second pathway commences with the splitting of a C—H bond, followed by a sequential hydrogen elimination process resulting in the production of CO. In Table 6, you can find the reaction energies and energy barriers for each elementary reaction, and figure 6 displays the

relevant transition states (TS). Exploring the sequential hydrogen elimination of other intermediate entities, we can propose and interpret four possible paths, as depicted in figure 4. The initial states (IS) for this hydrogen elimination process are selected being most steady adsorption configurations of the respective entities (figure 1), and the end states (FS) involve the co-adsorption of the hydrogen atom and the corresponding product entities in the most advantageous sites (figure 3). All reaction routes commence with CH<sub>3</sub>OH adsorbed at the t Pd site, traverse through co-adsorption configurations occupying strategically realistic positions, and culminate in the formation

of CO+H, where CO is anchored by adjacent bridge sites and H is bonded to the hollow site. These reactions are detailed in Table 4.

### 3.3.1. First pathway initiates with the breaking of the O—H bond

The breaking of the O—H bond of methanol is followed by the elimination of methylidyne H. Table 5 collects the frequency values connected to transition states, as well as the reaction energies and activation barriers for all elementary processes. Additionally, figure 5 provides visual representations of the pertinent transition states (TS) for these elementary reactions.



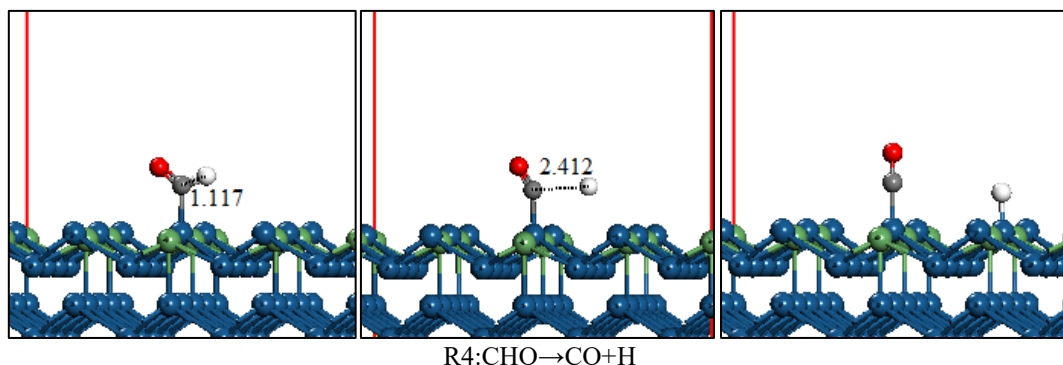


**Figure 5.** Schematic side of the initial state (IS), transition state (TS), and final states (FS) for CH<sub>3</sub>OH dehydrogenation via initial O—H scission on the PtGe(110) surface. (The bond length in (Å))

**Table 5.** The activation energy  $E_a$ (eV), the reaction energy  $E_r$ (eV) and the imaginary frequency ( $\text{cm}^{-1}$ ) of transition state for CH<sub>3</sub>OH dehydrogenation via O—H scission on the PtGe(110) surface.

Elementary reaction	$E_r$ (eV)	$E_a$ (eV)	Freq( $\text{cm}^{-1}$ )
R1:CH <sub>3</sub> OH→CH <sub>3</sub> O+H	- 0.178	0.924	-1203.0
R2:CH <sub>3</sub> O→CH <sub>2</sub> O+H	- 0.028	1.292	-57.9
R3:CH <sub>2</sub> O→CHO+H	- 0.128	1.329	-1031.9
R4:CHO→CO+H	- 0.637	1.302	-777.7

In the initial O—H bond scission, the activated O—H bond is elongated to 1.458 Å from 0.990 Å, and a Pt—H bond is formed in the final state FS. Additionally, the produced CH<sub>3</sub>O intermediate rotates to bind to its stable position (figure 5). The reaction is exothermic by -0.178 eV and the corresponding activation energy is 0.924 eV (Table 5), which is lower than that (1.472 eV) on the pure Pt(111) surface [52]. However, the extraction of methyl H from CH<sub>3</sub>O is easy, with a low activation barrier equal to 1.292 eV, and the reaction is exothermic by -0.028 eV (Table 5). It is clear that CH<sub>3</sub>O should rapidly decompose to CH<sub>2</sub>O on the surface of PtGe(110). During this process, the abstracted hydrogen is transferred to the top site of Pt, causing the C—H bond to elongate from 1.113 Å to 2.611 Å in the transition state (TS). After the formation of the TS, the oxygen atom remains bonded to its position on the top site  $t_{\text{Ge}}$ , and the O—C bond rotates to allow the carbon atom to bond to the top site  $t_{\text{Pt}}$ . Finally, the intermediate species CH<sub>2</sub>O adsorbs on the site adjacent to the preferred site of the hydrogen atom. Further decomposition of CH<sub>2</sub>O leads to the co-adsorption of CHO and H,

IS5

TS5

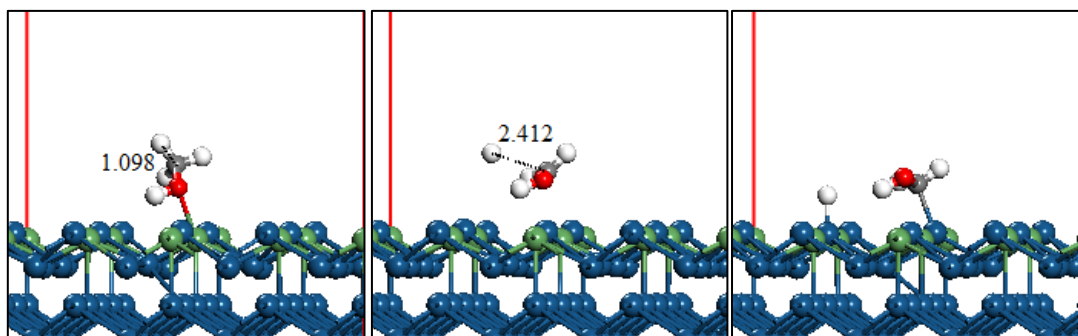
FS5

with an energy loss of - 0.128 eV and an energy barrier of 1.329 eV. This process involves the rotation of the C—O bond, which causes the Ge—O bond to break, on the other hand, the C—H bond breaks such that the distance  $d_{\text{C-H}} = 2.093$  Å in TS. After the TS the extracted H atom binds to the surface Pt atom, resulting in the adsorption of CHO to the top site Pt via the carbon atom. The subsequent abstraction of H from CHO forms the final product atomic CO and H. The process is exothermic by - 0.128 eV, with an activation barrier of 1.302 eV.

### 3.3.2. Second pathway initiates with the breaking of the C—H bond

The breaking of the C—H bond of methanol is followed by the elimination of methylidyne H. Table 6 compiles the reaction energies, activation barriers for all elementary reactions, and the frequency values associated with transition states. Additionally, figure 6 provides visual representations of the pertinent transition states (TS) for these elementary reactions.

Abdellatif Hassak, Rachida Ghailane

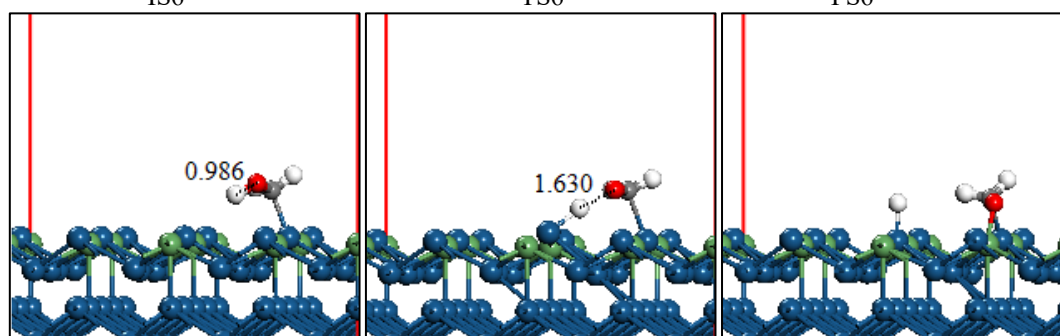


IS6

R5:  $\text{CH}_3\text{OH} \rightarrow \text{CH}_2\text{OH} + \text{H}$

TS6

FS6

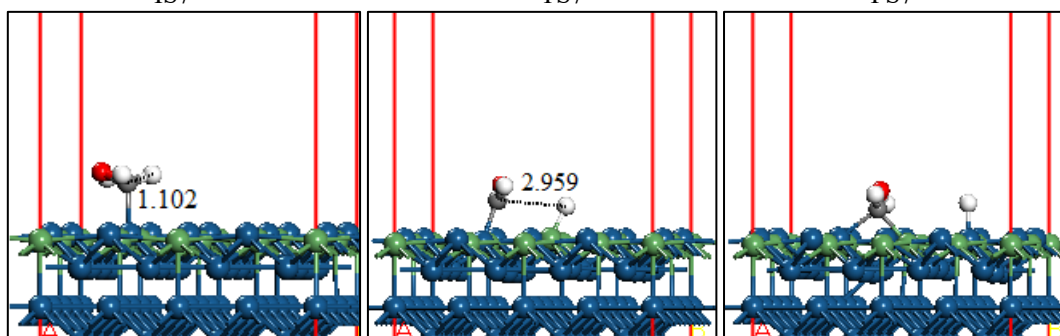


IS7

R6:  $\text{CH}_2\text{OH} \rightarrow \text{CH}_2\text{O} + \text{H}$

TS7

FS7

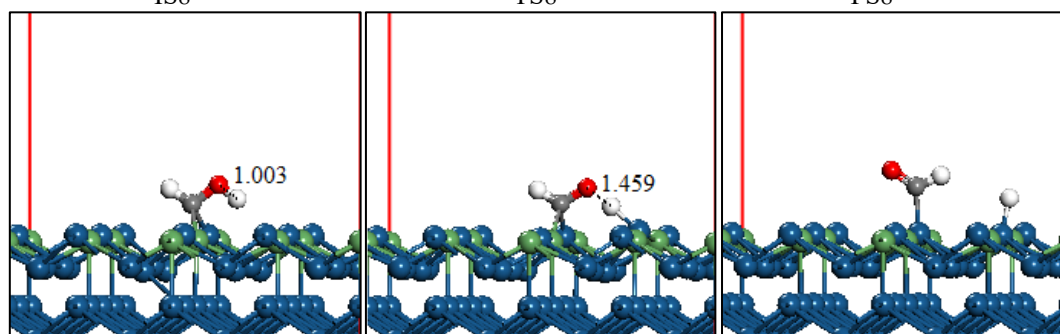


IS8

R7:  $\text{CH}_2\text{OH} \rightarrow \text{CHOH} + \text{H}$

TS8

FS8



IS9

R8:  $\text{CHOH} \rightarrow \text{CHO} + \text{H}$

TS9

FS9

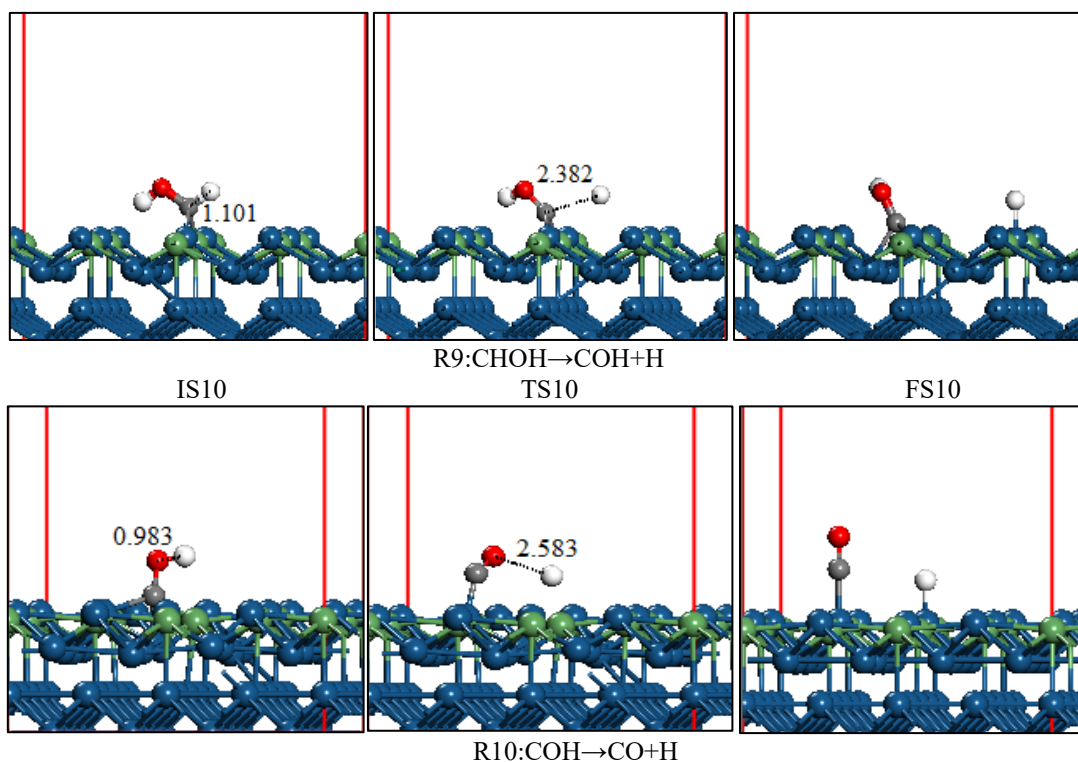


**Figure 6.** Schematic side of the initial state (IS), transition state (TS), and final states (FS) for  $\text{CH}_3\text{OH}$  dehydrogenation via initial C—H scission on the PtGe(110) surface. (The bond length in (Å))

**Table 6.** The activation energy  $E_a$ (eV), the reaction energy  $E_r$ (eV) and the imaginary frequency ( $\text{cm}^{-1}$ ) of transition state for  $\text{CH}_3\text{OH}$  dehydrogenation via C—H scission on the PtGe(110) surface.

Elementary reaction	$E_r$ (eV)	$E_a$ (eV)	Freq( $\text{cm}^{-1}$ )
R5: $\text{CH}_3\text{OH} \rightarrow \text{CH}_2\text{OH} + \text{H}$	- 0.151	3.237	- 865.2
R6: $\text{CH}_2\text{OH} \rightarrow \text{CH}_2\text{O} + \text{H}$	0.035	0.984	- 200.7
R7: $\text{CH}_2\text{OH} \rightarrow \text{CHOH} + \text{H}$	0.189	1.649	- 530.4
R8: $\text{CHOH} \rightarrow \text{CHO} + \text{H}$	- 0.275	0.711	- 486.1
R9: $\text{CHOH} \rightarrow \text{COH} + \text{H}$	0.509	2.003	- 995.2
R10: $\text{COH} \rightarrow \text{CO} + \text{H}$	-1.063	1.071	-897.9

The initial activation of the C-H bond on PtGe(110) begins with a tilt of the adsorbed methanol so that the methyl group can descend until the O—C bond becomes nearly parallel to the surface, allowing one of the C—H bonds to be activated. In TS, the activated C—H bond is elongated to 2.412 Å from 1.098 Å (figure 6). After TS, the H atom moves to a top site of Pt, and the Pt—C distance is further shortened, allowing  $\text{CH}_2\text{OH}$  to form a bond from the C atom to the bridge site of Pt, its stable configuration as FS. This process is exothermic by -0.151 eV and undergoes an energy barrier of 3.237 eV (Table 6). This barrier is higher than that of the O—H separation, indicating on PtGe(110) that the separation of the O—H bond of  $\text{CH}_3\text{OH}$  is more favorable.

In the dehydrogenation of  $\text{CH}_2\text{OH}$  on the surface of PtGe(110), two pathways are predicted:  $\text{CH}_2\text{OH} \rightarrow \text{CH}_2\text{O} + \text{H}$  and  $\text{CH}_2\text{OH} \rightarrow \text{CHOH} + \text{H}$ , starting from the stable position occupied by  $\text{CH}_2\text{OH}$  at the site  $t_{\text{Pt}}$ . In the case of O—H bond scission via the  $\text{CH}_2\text{OH} \rightarrow \text{CH}_2\text{O} + \text{H}$  process, the O—H bond is broken, causing  $\text{CH}_2\text{O}$  to adsorb on  $t_{\text{Pt}}-t_{\text{Ge}}$  with a bond of C to the Pt atom, and O bonded to the Ge atom, with H occupying the neighboring top site of Pt. In (TS6) (figure 6). The surface of PtGe(110) and the C—O bond axis of  $\text{CH}_2\text{O}$  are almost parallel. The separation of the O atom from the dissociated H atom is increased to 1.630 Å. This simple reaction has an endothermic energy of 0.035 eV and needs to overcome the energy barrier of 0.984 eV. The reaction  $\text{CH}_2\text{OH} \rightarrow$

CHOH + H, occurs when the C—H bond breaks rather than the O—H bond leading to the creation of CHOH. In fact, the H atom attached to the C atom travels toward the surface, stretching the C—H bond to 2.959 Å (TS7.R7) (figure 6). Finally, the obtained CHOH is co-adsorbed on the PtGe(110) surface with the H atom is also adsorbed at the top site Pt. This step necessity 1.649 eV as the activation barrier and a reaction energy of 0.189 eV. Therefore, from the comparison of the energy barrier and reaction energy values, it is clear that the O—H bond cleavage of CH<sub>2</sub>OH is slightly favorable, which means, CH<sub>2</sub>OH prefers cleavage of the O—H bond to produce CH<sub>2</sub>O rather than cleavage of the C—H bond, which leads to CHOH.

In The dissociation of CHOH, two possible reactions on the surface of PtGe(110) are examined: the cleavage of the OH bond to CHO and the cleavage of the C—H bond to COH. In the CHOH→CHO+H reaction, CHOH stably binds to bridged sites ( $b_{PtGe}$ ) on PtGe(110). In the transition state (TS8) (figure 6), the dissociated H always localizes to the top site t-Pt with a slight inclination. Subsequently, CHO extends further to the most stable site on the top site of Pt, by the splitting of the C—Ge bond, while turning and the H atom moves to the top site of Pt, reaching the FS with an exothermic energy equal to - 0.275 eV. The activation barrier of this process is determined at 0.711 eV. COH is formed via C—H bond scission for the reaction CHOH → COH + H. A distance of 2.382 Å is found between the dissociated H atom and the C atom in TS9 (figure 6). For the final state, COH binds to the hollow site  $h_{Pt2Ge}$  through its carbon atom, and the dissociated H atom is located at the adjacent top site  $t_{Pt}$ . This reaction has an energy barrier of 2.003eV and an endothermic energy of 0.509eV. Then it is obvious that CHOH prefers the O—H bond cleavage. The subsequent abstraction of H from COH forms the final product atomic CO and H. The process is exothermic by - 0.091 eV, with an activation barrier of 1.052 eV.

The most favorable adsorption position ( $h_{Pt2Ge}$ ) is chosen as the initial state in the case of the dehydrogenation of COH. Afterward, COH dissociates to produce CO and H by breaking the OH bond. The interatomic distance between the dissociated H atom and the O atom increases to reach 2.583 Å (TS10.R10) figure 6, Subsequently, CO occupies the  $t_{Pt}$  site while H is bound to the adjacent  $t_{Pt}$  site. This elementary reaction must cross an energy barrier of 1.071eV and reaction energy of -1.063 eV (exothermic process). It is also noticeable that the O—H scission is kinetically and thermodynamically more favorable than the C—H one overall the pathways of dehydrogenation.

#### 4. Conclusions

In summary, a combination of partial density of states calculations, electronic configuration, and Mulliken atomic charges reveals that the interaction between Pt and CO is weakened in the presence of Ge. This indicates that the alloy of Pt with Ge leads to more stable catalysts with greater resistance to deactivation via CO poisoning. This is attributed to compromised availability of Pt d orbitals due to covalence interactions with Ge, thereby hindering the Pt→CO 2π back-donation step.

The DFT-D study of the methanol dehydrogenation reaction network on the PtGe(110) surface involves reactions describing the cleavage of O—H and C—H bonds according to two modes. The study controls structural parameters and energetic characteristics of the intermediates. Results show that initial cleavage of the O—H bond of CH<sub>3</sub>OH is preferred on the PtGe(110) surface due to a lower activation barrier and exothermic reaction energy.

A systematic comparison of four different reaction pathways demonstrates that the hydrogen production chain CH<sub>3</sub>OH → CH<sub>3</sub>O → CH<sub>2</sub>O → CHO → CO is the most kinetically favorable during methanol dehydrogenation on the PtGe(110) surface.

In conclusion, this study enhances our understanding of the dehydrogenation process on PtGe bimetallic catalysts, offering insights for predicting the design of DMFC electrodes with long-term efficiency and performance.

#### References

- [1] M. AlKhars, F. Miah, H. Qudrat-Ullah, A. Kayal, A Systematic Review of the Relationship Between Energy Consumption and Economic Growth in GCC Countries, Sustainability. 12 (2020) 3845.
- [2] A. Karki, S. Phuyal, D. Tuladhar, S. Basnet, B. Shrestha, Status of Pure Electric Vehicle Power Train Technology and Future Prospects, ASI. 3 (2020) 35.
- [3] X. Pan, H. Wang, L. Wang, W. Chen, Decarbonization of China's transportation sector: In light of national mitigation toward the Paris Agreement goals, Energy. 155 (2018) 853–864.
- [4] G. Xu, R. Si, J. Liu, L. Zhang, X. Gong, R. Gao, B. Liu, J. Zhang, Directed self-assembly pathways of three-dimensional Pt/Pd nanocrystal superlattice electrocatalysts for enhanced methanol

- oxidation reaction, J. Mater. Chem. A. 6 (2018) 12759–12767.
- [5] S.S. Munjewar, S.B. Thombre, Effect of current collector roughness on performance of passive direct methanol fuel cell, Renew. Energy 138 (2019) 272–283.
- [6] H. Li, Q. Fu, L. Xu, S. Ma, Y. Zheng, X. Liu, S. Yu, Highly crystalline PtCu nanotubes with three dimensional molecular accessible and restructured surface for efficient catalysis, Energy Environ. Sci. 10 (2017) 1751–1756.
- [7] S. Şen, F. Şen, G. Gökağaç, Preparation and characterization of nano-sized Pt–Ru/C catalysts and their superior catalytic activities for methanol and ethanol oxidation, Phys. Chem. Chem. Phys. 13 (2011) 6784.
- [8] F. Şen, G. Gökağaç, Improving Catalytic Efficiency in the Methanol Oxidation Reaction by Inserting Ru in Face-Centered Cubic Pt Nanoparticles Prepared by a New Surfactant, *tert*-Octanethiol, Energy Fuels. 22 (2008) 1858–1864.
- [9] Y. Yıldız, S. Kuzu, B. Sen, A. Savk, S. Akocak, F. Şen, Different ligand based monodispersed Pt nanoparticles decorated with rGO as highly active and reusable catalysts for the methanol oxidation, International Journal of Hydrogen Energy. 42 (2017) 13061–13069.
- [10] S. Papadimitriou, S. Armanyanov, E. Valova, A. Hubin, O. Steenhaut, E. Pavlidou, G. Kokkinidis, S. Sotiropoulos, Methanol Oxidation at Pt–Cu, Pt–Ni, and Pt–Co Electrode Coatings Prepared by a Galvanic Replacement Process, J. Phys. Chem. C. 114 (2010) 5217–5223.
- [11] F. Sen, Y. Karatas, M. Gulcan, M. Zahmakiran, Amylamine stabilized platinum(0) nanoparticles: active and reusable nanocatalyst in the room temperature dehydrogenation of dimethylamine-borane, RSC Adv. 4 (2014) 1526–1531.
- [12] L. Liu, E. Pippel, R. Scholz, U. Gösele, Nanoporous Pt–Co Alloy Nanowires: Fabrication, Characterization, and Electrocatalytic Properties, Nano Lett. 9 (2009) 4352–4358.
- [13] B. Çelik, S. Kuzu, E. Erken, H. Sert, Y. Koşkun, F. Şen, Nearly monodisperse carbon nanotube furnished nanocatalysts as highly efficient and reusable catalyst for dehydrocoupling of DMAB and C1 to C3 alcohol oxidation, International Journal of Hydrogen Energy. 41 (2016) 3093–3101.
- [14] F. Vigier, S. Rousseau, C. Coutanceau, J.-M. Leger, C. Lamy, Electrocatalysis for the direct alcohol fuel cell, Top Catal. 40 (2006) 111–121.
- [15] Z. Yang, Y. Shi, X. Wang, G. Zhang, P. Cui, Boron as a superior activator for Pt anode catalyst in direct alcohol fuel cell, Journal of Power Sources. 431 (2019) 125–134.
- [16] J.C. Park, C.H. Choi, Graphene-derived Fe/Co-N-C catalyst in direct methanol fuel cells: Effects of the methanol concentration and ionomer content on cell performance, Journal of Power Sources. 358 (2017) 76–84.
- [17] E. Antolini, J.R.C. Salgado, E.R. Gonzalez, The stability of Pt–M (M=first row transition metal) alloy catalysts and its effect on the activity in low temperature fuel cells, Journal of Power Sources. 160 (2006) 957–968.
- [18] T. Hyeon, S. Han, Y.-E. Sung, K.-W. Park, Y.-W. Kim, High-Performance Direct Methanol Fuel Cell Electrodes using Solid-Phase-Synthesized Carbon Nanocoils, Angew. Chem. 115 (2003) 4488–4492.
- [19] Y. Mu, H. Liang, J. Hu, L. Jiang, L. Wan, Controllable Pt Nanoparticle Deposition on Carbon Nanotubes as an Anode Catalyst for Direct Methanol Fuel Cells, J. Phys. Chem. B. 109 (2005) 22212–22216.
- [20] F. Şen, G. Gökağaç, S. Şen, High performance Pt nanoparticles prepared by new surfactants for C1 to C3 alcohol oxidation reactions, J Nanopart Res. 15 (2013) 1979.
- [21] J. Qi, S. Yan, Q. Jiang, Y. Liu, G. Sun, Improving the activity and stability of a Pt/C electrocatalyst for direct methanol fuel cells, Carbon. 48 (2010) 163–169.
- [22] E. Erken, İ. Esirden, M. Kaya, F. Sen, A rapid and novel method for the synthesis of 5-substituted 1H-tetrazole catalyzed by exceptional reusable monodisperse Pt NPs@AC under the microwave irradiation, RSC Adv. 5 (2015) 68558–68564.

- [23] C. Li, H. Tan, J. Lin, X. Luo, S. Wang, J. You, Y.-M. Kang, Y. Bando, Y. Yamauchi, J. Kim, Emerging Pt-based electrocatalysts with highly open nanoarchitectures for boosting oxygen reduction reaction, *Nano Today*. 21 (2018) 91–105.
- [24] C. Li, M. Iqbal, J. Lin, X. Luo, B. Jiang, V. Malgras, K.C.-W. Wu, J. Kim, Y. Yamauchi, Electrochemical Deposition: An Advanced Approach for Templated Synthesis of Nanoporous Metal Architectures, *Acc. Chem. Res.* 51 (2018) 1764–1773.
- [25] H. Atae-Esfahani, J. Liu, M. Hu, N. Miyamoto, S. Tominaka, K.C.W. Wu, Y. Yamauchi, Mesoporous Metallic Cells: Design of Uniformly Sized Hollow Mesoporous Pt-Ru Particles with Tunable Shell Thicknesses, *Small*. 9 (2013) 1047–1051.
- [26] C. Li, M. Iqbal, B. Jiang, Z. Wang, J. Kim, A.K. Nanjundan, A.E. Whitten, K. Wood, Y. Yamauchi, Pore-tuning to boost the electrocatalytic activity of polymeric micelle-templated mesoporous Pd nanoparticles, *Chem. Sci.* 10 (2019) 4054–4061.
- [27] H. Atae-Esfahani, L. Wang, Y. Yamauchi, Block copolymer assisted synthesis of bimetallic colloids with Au core and nanodendritic Pt shell, *Chem. Commun.* 46 (2010) 3684.
- [28] E. Kuyuldar, H. Burhan, A. Şavk, B. Güven, C. Özdemir, S. Şahin, A. Khan, F. Şen, Enhanced Electrocatalytic Activity and Durability of PtRu Nanoparticles Decorated on rGO Material for Ethanol Oxidation Reaction, in: A. Khan, M. Jawaid, B. Neppolian, A.M. Asiri (Eds.), *Graphene Functionalization Strategies*, Springer Singapore, Singapore, 2019: pp. 389–398.
- [29] S. Stevanović, D. Tripković, A. G. Wohlmuther, J. Rogan, U. Lačnjevac, V. Jovanović, Carbon Supported PtSn versus PtSnO<sub>2</sub> Catalysts in Methanol Oxidation, *Int. J. Electrochem. Sci.* 16 (2021) 1-16.
- [30] H. Tian, Y. Yu, Q. Wang, J. Li, P. Rao, R. Li, Y. Du, C. Jia, J. Luo, P. Deng, Y. Shen, X. Tian, Recent advances in two-dimensional Pt based electrocatalysts for methanol oxidation reaction, *International Journal of Hydrogen Energy*. 46 (2021) 31202–31215.
- [31] L. Chen, L. Zhou, H. Lu, Y. Zhou, J. Huang, J. Wang, Y. Wang, X. Yuan, Y. Yao, Shape-controlled synthesis of planar PtPb nanoplates for highly efficient methanol electro-oxidation reaction, *Chem. Commun.* 56 (2020) 9138–9141.
- [32] Q. Lv, X. Ren, L. Liu, W. Guan, A. Liu, Theoretical investigation of methanol oxidation on Pt and PtNi catalysts, *Ionics*. 26 (2020) 1325–1336.
- [33] G. You, J. Jiang, M. Li, L. Li, D. Tang, J. Zhang, X.C. Zeng, R. He, PtPd(111) Surface versus PtAu(111) Surface: Which One Is More Active for Methanol Oxidation?, *ACS Catal.* 8 (2018) 132–143.
- [34] P. Wang, H. Cui, C. Wang, Ultrathin PtMo-CeO hybrid nanowire assemblies as high-performance multifunctional catalysts for methanol oxidation, oxygen reduction and hydrogen oxidation, *Chemical Engineering Journal*. 429 (2022) 132435.
- [35] C. Li, M. Iqbal, J. Lin, X. Luo, B. Jiang, V. Malgras, K.C.-W. Wu, J. Kim, Y. Yamauchi, Electrochemical Deposition: An Advanced Approach for Templated Synthesis of Nanoporous Metal Architectures, *Acc. Chem. Res.* 51 (2018) 1764–1773.
- [36] E. Jimenez-Izal, J.-Y. Liu, A.N. Alexandrova, Germanium as key dopant to boost the catalytic performance of small platinum clusters for alkane dehydrogenation, *Journal of Catalysis*. 374 (2019) 93–100.
- [37] A. Ugartemendia, K. Peeters, P. Ferrari, A. Cózar, J.M. Mercero, E. Janssens, E. Jimenez-Izal, Doping Platinum with Germanium: An Effective Way to Mitigate the CO Poisoning, *ChemPhysChem*. 22 (2021) 1603–1610.
- [38] N.S. Veizaga, V.I. Rodriguez, M. Bruno, S.R. de Miguel, The Role of Surface Functionalities in PtGe and PtIn Catalysts for Direct Methanol Fuel Cells, *Electrocatalysis*. 10 (2019) 125–133.
- [39] N.S. Veizaga, V.A. Paganin, T.A. Rocha, O.A. Scelza, S.R. de Miguel, E.R. Gonzalez, Development of PtGe and PtIn anodic catalysts supported on carbonaceous materials for DMFC, *International Journal of Hydrogen Energy*. 39 (2014) 8728–8737.

- [40] B. Delley, From molecules to solids with the DMol3 approach, *The Journal of Chemical Physics*. 113 (2000) 7756–7764.
- [41] B. Delley, An all-electron numerical method for solving the local density functional for polyatomic molecules, *The Journal of Chemical Physics*. 92 (1990) 508–517.
- [42] J.P. Perdew, K. Burke, M. Ernzerhof, Generalized Gradient Approximation Made Simple, *Phys. Rev. Lett.* 77 (1996) 3865–3868.
- [43] H.J. Monkhorst, J.D. Pack, Special points for Brillouin-zone integrations, *Phys. Rev. B*. 13 (1976) 5188–5192.
- [44] S. Grimme, Semiempirical GGA-type density functional constructed with a long-range dispersion correction, *J. Comput. Chem.* 27 (2006) 1787–1799.
- [45] S. Grimme, Density functional theory with London dispersion corrections, *WIREs Comput Mol Sci*. 1 (2011) 211–228.
- [46] T.A. Halgren, W.N. Lipscomb, The synchronous-transit method for determining reaction pathways and locating molecular transition states, *Chemical Physics Letters*. 49 (1977) 225–232.
- [47] Z. Jiang, B. Wang, T. Fang, Adsorption and dehydrogenation mechanism of methane on clean and oxygen-covered Pd (1 0 0) surfaces: A DFT study, *Applied Surface Science*. 320 (2014) 256–262.
- [48] M.D. Esrafil, R. Nurazar, A DFT study on the possibility of using boron nitride nanotubes as a dehydrogenation catalyst for methanol, *Applied Surface Science*. 314 (2014) 90–96.
- [49] P. Du, P. Wu, C. Cai, Mechanism of Methanol Decomposition on the Pt<sub>3</sub>Ni(111) Surface: DFT Study, *J. Phys. Chem. C*. 121 (2017) 9348–9360.
- [50] T. Choksi, J. Greeley, Partial Oxidation of Methanol on MoO<sub>3</sub> (010): A DFT and Microkinetic Study, *ACS Catal.* 6 (2016) 7260–7277.
- [51] W. Zhang, G.-J. Xia, Y.-G. Wang, Mechanistic insight into methanol electro-oxidation catalyzed by PtCu alloy, *Chinese Journal of Catalysis*. 43 (2022) 167–176.
- [52] X. Wang, W.-K. Chen, C.-H. Lu, A periodic density functional theory study of the dehydrogenation of methanol over CuCl(111) surface, *Applied Surface Science*. 254 (2008) 4421–4431.
- [53] L. Zhao, S. Wang, Q. Ding, W. Xu, P. Sang, Y. Chi, X. Lu, W. Guo, The Oxidation of Methanol on PtRu(111): A Periodic Density Functional Theory Investigation, *J. Phys. Chem. C*. 119 (2015) 20389–20400.
- [54] X. Wang, L. Chen, B. Li, A density functional theory study of methanol dehydrogenation on the PtPd<sub>3</sub>(111) surface, *International Journal of Hydrogen Energy*. 40 (2015) 9656–9669.
- [55] A. Hassak, R. Ghailane, Theoretical investigation of the hydrogen production by adsorption of methanol on bimetallic Pd-Ge (1 1 0) surface as future green combustible using DFT-D method: Energetic and structural aspect of interaction pathways of metal with methanol, *Computational and Theoretical Chemistry*. 1210 (2022) 113635.
- [56] R. Jiang, W. Guo, M. Li, X. Lu, J. Yuan, H. Shan, Dehydrogenation of methanol on Pd(100): comparison with the results of Pd(111), *Phys. Chem. Chem. Phys.* 12 (2010) 7794–7803.
- [57] K.W. Park, J.H. Choi, Y.E. Sung, Structural, chemical, and electronic properties of Pt/Ni thin film electrodes for methanol electrooxidation, *J. Phys. Chem. B* 107 (2003) 5851–5856.
- [58] Y. Ishikawa, M.S. Liao, C.R. Cabrera, Oxidation of methanol on platinum, ruthenium and mixed Pt–M metals (M = Ru, Sn): a theoretical study, *Surf. Sci.* 463 (2000) 66–80.